

Numerical assessment of post-tensioned slab-edge column connection systems with and without shear cap

Farshad Janghorban^{*1} and Abdollah Hoseini^{2a}

¹Civil Engineering Department, Kish International Campus, University of Tehran, Niyayesh St., Mirmohanna Blvd., Kish Island, Iran

²Civil Engineering Department, University of Tehran, 16th Azar St., Enghelab Sq., Tehran, Iran

(Received January 23, 2018, Revised April 22, 2018, Accepted April 28, 2018)

Abstract. Introduction of prestressed concrete slabs based on post-tensioned (PT) method aids in constructing larger spans, more useful floor height, and reduces the total weight of the building. In the present paper, for the first time, simulation of 32 two-way PT slab-edge column connections is performed and verified by some existing experimental results which show good consistency. Finite element method is used to assess the performance of bonded and unbonded slab-column connections and the impact of different parameters on these connections. Parameters such as strand bonding conditions, presence or absence of a shear cap in the area of slab-column connection and the changes of concrete compressive strength are implied in the modeling. The results indicate that the addition of a shear cap increases the flexural capacity, further increases the shear strength and converts the failure mode of connections from shear rigidity to flexural ductility. Besides, the reduction of concrete compressive strength decreases the flexural capacity, further reduces the shear strength of connections and converts the failure mode of connections from flexural ductility to shear rigidity. Comparing the effect of high concrete compressive strengths versus the addition of a shear cap, shows that the latter increases the shear capacity more significantly.

Keywords: prestressed concrete slab; post-tensioned; shear cap; unbonded; bonded

1. Introduction

The advent of prestressing concrete structures has led to significant change in the design, implementation and accurate performances of reinforced concrete structures, especially for constructing large spans in concrete buildings. The application of prestressing force is done in two ways: one is pre-tensioned method where tendons are tensioned prior to concrete casting; the other is post-tensioned (PT) method where tendons are tensioned after concrete casting. In the latter, i.e., PT method, the tendons should not be bonded to the concrete, otherwise they cannot be tensioned; that is why PT tendons are placed inside ducts. Implementation of such a ceiling system is possible with the use of two types of unbonded and bonded tendons.

One of the main problems of PT slab-column connections is the emergence of cracks around the connection areas and the failure caused by punching shear that requires further investigations into the seismic performance and ductility of connections, despite the ACI 318 building code requirements for their reduction. More fundamental studies is essential due to the lack of comprehensive experiments on a variety of connection types and the limited reports on comparing two types of connections with unbonded and bonded tendons. A few

experiments that compared unbonded and bonded tendons in PT members include investigations of Mattock *et al.* (1971) into a set of PT beams with unbonded and bonded tendons to assess their ultimate moment strength and Cooke *et al.*'s (1981) studies on 12 one-way slabs with unbonded and bonded tendons to assess their flexural strength.

To the best of the authors' knowledge, no experiment has been done yet to compare the effect of the presence or absence of unbonded and bonded tendons on two-way slabs or slab-column connections (Kang *et al.* 2015). Due to some limitations of ACI 318-14 building code requirements on the implementation of such ceiling systems (ACI 318-14 2014), the significance and necessity of developing a more precise and reliable simulation model to verify the validity of the questioned experiments is felt more than ever.

A limited number of investigations have been done into two-way unbonded PT slab-edge column connections by Trongtham and Hawkins (1977) who tested one unbonded slab-edge column connection. The slab was loaded vertically at two points, one in the vicinity of column and the other at a greater distance from the column. This loading pattern was aimed to apply the desired moment shear ratio to the test specimen. The results showed that the ACI 318-71 building code requirements and regulations were applicable to the design of the PT slab-edge column connection. Sunidja *et al.* (1982) studied four unbonded two-way PT slab edge-column connections. Their results indicated that ACI 318-83 building code limitations on maximum values of concrete compressive strength are not necessary. Dilger and Shatila (1989) intended to investigate the effect of the presence of overhangs and shear studs on six unbonded PT slab-edge column connections. The results

*Corresponding author, M.Sc. Student

E-mail: f.janghorban@ut.ac.ir

^aAssociate Professor

E-mail: hoseiniaby@ut.ac.ir

indicated that the ACI 318-83 building code requirements and regulations were conservative in calculating the shear strength of slab-edge column connections.

Martinez-Cruzado (1993) tested two unbonded column connections. The specimens of this experiment used roller supports on the edge of slabs, and hinges on the bottom of columns. The results showed that the ACI 318-89 building code requirements and regulations were acceptable for calculating the shear strength of PT slab-edge column connections. According to Martinez-Cruzado, the presence of high compressive stresses in the area of slab-column connections increased the strength of connections when the reinforcing bars of slabs were close to the tensile slabs surface. Han *et al.* (2006) explored two unbonded PT slab-edge column connections. This experiment used hinge supports on both edges of slabs and hinges on the top and bottom of columns. According to the results, the distributed tendons arrangement had greater impacts on lateral drift capacity, hysteretic energy dissipation capacity and PT slabs-edge column connections than banded tendons arrangement.

Furthermore, Huang (2012) introduced two methods of contact formulation and spring system for simulating PT members in Abaqus finite element analysis (FEA) software. Huang *et al.* (2010), Kang and Huang (2012), Kim *et al.* (2014) studied three modeling approaches to simulate unbonded conditions in Abaqus software. Kang *et al.* (2015) used the developed modeling techniques to provide a comparison between concrete members with different tendon systems. Kwak *et al.* (2006) demonstrated a tendon model that can effectively be used in FEA of prestressed concrete structures by considering slip behavior of tendons. Yapar *et al.* (2015) presented a finite element (FE) model for pre-tensioned prestressed concrete beams. Abdelatif *et al.* (2015) developed three models to simulate the transfer of prestress force from steel to concrete in pre-tensioned concrete elements. Abdullah *et al.* (2016) investigated a FE model of prestressed strand for a detailed analysis of its mechanical behavior. Bílý and Kohoutková (2017) suggested a numerical analysis of the stress-strain behavior of the steel liner of a prestressed concrete containment wall. Hajali *et al.* (2015) used a FEA model to assess the impact of the location of broken prestressed wire wraps on the overall strength of prestressed concrete cylinder pipes. Brunesi *et al.* (2015) proposed a modeling approach based on non-linear fracture mechanisms to predict the shear performance of precast-prestressed hollow core slabs. Zobel and Curbach (2017) modeled the reinforced and prestressed concrete containment wall under biaxial tensile stresses. Several studies offered a FE model to simulate non-linear structural behavior of PT composite beams with partial shear connectors (Hwang *et al.* 2014) and prestressed continuous composite beams (Nie *et al.* 2011).

This study presents the simulation of 32 two-way PT slab-edge column connections which is verified with the experimental results of Cooke *et al.* (1981) and Sunidja *et al.* (1982), based on contact formulation method developed by Huang (2012). The novelty of this work is the addition of a shear cap in the area of slab-column connection, reduction of concrete compressive strength and the change of strand bonding conditions from unbonded to bonded and

its effect on the lateral performance of PT slab-edge column connections.

2. Numerical modeling of unbonded and bonded PT slabs

This section presents the simulation of unbonded and bonded PT slabs in detail in Abaqus FEA software including an introduction to the characteristics of materials, elements, and constraints used in modeling.

2.1 Concrete modeling

In order to consider the damages and cracking of concrete in Abaqus, damaged plasticity model was used for nonlinear dynamic analyses which assumes two main premises in failure mechanism: one is tensile cracking, and the other is compressive crushing.

Damaged plasticity model requires a uniaxial stress-strain relation for concrete under compression to be defined and a tensile stiffening model to be used. The empirical model proposed by Carreira and Chu (1985) for the compression behavior of concrete was employed, which is given in Eqs. (1) to (3)

$$\frac{f_c}{f'_c} = \frac{\beta \left(\frac{\epsilon}{\epsilon'_c}\right)}{\beta - 1 + \left(\frac{\epsilon}{\epsilon'_c}\right)^\beta} \quad (1)$$

$$\beta = \frac{1}{1 - \left[\frac{f'_c}{\epsilon'_c E_{it}}\right]} \quad (2)$$

$$\epsilon'_c = (0.71f'_c + 168) \times 10^{-5} \quad (3)$$

The required value of E_{it} in Eq. (2) was obtained through the equation proposed by Nilson *et al.* (2009).

$$E_{it} = (3320 \sqrt{f'_c} + 6900) \left(\frac{w_c}{2300}\right)^{1.5} \quad (4)$$

Where f_c (MPa) is concrete compressive stress (variable); f'_c (MPa) is concrete compressive strength; ϵ'_c is concrete strain corresponding to f'_c ; ϵ is concrete compressive strain corresponding to f_c (variable); E_{it} (MPa) is initial tangent modulus of elasticity; and w_c ($\frac{kg}{m^3}$) is unit weight of the concrete.

In the tensile stiffening model used in the current study, the cracking strain was considered twice as much as that strain corresponding to f'_t . Fig. 1 displays the tensile

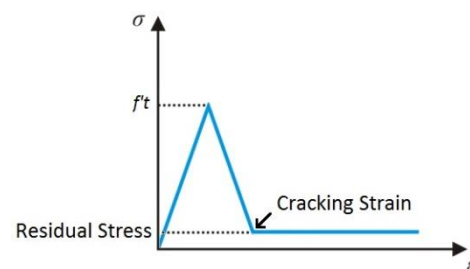


Fig. 1 Tensile stiffening model for concrete

stiffening model used for concrete. The value of f_t' was directly derived from laboratory data and the value of residual stress was assumed to be 10% of f_t' .

The value of dilation angle of concrete is about 20 to 50 degrees (Kang and Huang 2012). Basically, the smaller the angle, the more rigidity resulted, and the larger the angle the more ductility. In general, dilation angle such as 30 to 40 degrees is defined in the damaged plasticity model which was used in this work. Therefore, the value of dilation angle was chosen to be 30 degrees.

2.2 Bonded reinforcement and PT tendon modeling

In order to define a uniaxial stress-strain relation for the reinforcing bars, elastic-perfectly plastic model was used. Besides, a nonlinear plasticity model was also used to define a uniaxial stress-strain relation for PT tendons. This nonlinear relation was introduced using the stress-strain empirical model proposed by Devalapura and Tadros (1992) for grade 270 seven-wire strands which is described as follows

$$f_{ps} = 6.9\epsilon_{ps} \left[A + \frac{B}{(1 + (C\epsilon_{ps})^D)^{1/D}} \right] \leq 1862 \text{ MPa} \quad (5)$$

Where f_{ps} (MPa) is stress in tendon (variable) and ϵ_{ps} is strain in tendon (variable). The values of A , B , C , and D in Eq. (5) are constants equal to 887, 27613, 112.4 and 7.36 respectively.

2.3 Elements

Eight-node first-order element with reduced integration (C3D8R) is an appropriate simulation model for all concrete members, ducts and steel plates. The main advantage of this element is prevention of shear locking as the most fundamental problem in full integration elements. Shear locking results in excessive resistance against moments in the elements. That is why they should be replaced with elements with reduced integration such as C3D8R which has higher flexibility. However, it should be noted that if the used mesh generation is coarse, the results will be useless. Therefore, the accuracy of analysis should be maximized by mesh refinement. Two-node linear truss element (T3D2) was used for simulating the reinforcing bars and PT tendons.

2.4 Interaction between different parts of PT slabs

In order to define the interaction between the concrete and reinforcing bars, the embedded region constraint in Abaqus was used, which is able to constrain the translational degrees of freedom. Besides, embedded region constraint was also used to define the interactions between concrete and ducts.

The modeling of the end anchorage of PT tendons is possible through multi-point constraints (AKA MPCs) in Abaqus. The beam type of MPC constraint was used in this study that is able to constrain the displacement and rotation of any selected area by the tendon end nodes.

Contact formulation is an appropriate method for simulation of PT systems that has more flexibility and accuracy than other methods and allows modeling both bonding types i.e., unbonded and bonded modes for tendons. This method helps to create different contact modes between contact surfaces (i.e., the external surface of PT tendons element and the internal surface of their corresponding duct elements). The simulation of contact surfaces between PT tendons elements and their corresponding duct elements was done on a surface-to-surface contact basis in Abaqus. The tangential behavior could be selected as frictionless or rough. In the former case, i.e., frictionless, the tendons have the ability to slip in the prestressing step through which the unbonded mode is simulated. By changing the frictionless to rough after prestressing step, the system changes to a bonded one.

2.5 Modeling prestressing procedures

All modelings are based on the explicit dynamic analysis. The present study used the temperature field capability to apply the PT forces by decreasing the temperature of tendons. Such modeling has several steps. In the first step, the interaction between tendons and ducts should be considered frictionless as discussed earlier. Afterwards, the PT forces should be applied by decreasing the temperature of tendons. In the next step, the desired external loads should be applied.

3. Model verification

This section introduces the numerical models to verify the contact formulation method for the simulation of slabs with unbonded and bonded tendons. Then the simulation results were compared with the results of laboratory experiments.

3.1 One-way unbonded and bonded PT slabs

Cooke *et al.* (1981) tested twelve simply supported one-way PT slabs. Nine slabs had unbonded tendons and the remaining three slabs had bonded tendons. Amongst the tested specimens, both the Slab5 and Slab B5 specimens were selected for simulation in Abaqus. The diameter of tendons used in these specimens was 12.70 mm which were located in PVC ducts with a diameter of 14 mm. None of the slabs used reinforcing bars and the tendons were placed in a straight position in all specimens. All specimens of this experiment underwent linear vertical loadings in two areas of slabs until they failed. The dimensions of simulated slabs and position of two linear loads are displayed in Fig. 2. Table 1 presents the properties and details of both intended specimens. The properties of both the Slab 5 and Slab B5 specimens were similar to each other except for the strand bonding conditions of their tendons which differed. Therefore, after simulating the Slab 5 specimen with unbonded tendons, only the contact mode of its tendons changed from frictionless to rough for simulation of the Slab B5 specimen with bonded tendons after prestressing step.

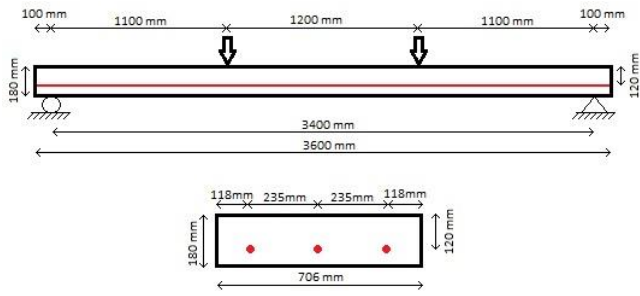


Fig. 2 Dimensions of the Slab 5 and Slab B5 specimens (Cooke *et al.* 1981, Huang 2012)

Table 1 Properties and details of the Slab 5 and Slab B5 specimens

Specimen	Section Properties			Material Properties			
	b , mm	h , mm	l , mm	f_c^i , MPa	f_t^i , MPa	f_{pu} , MPa	f_{se} , MPa
Slab 5	706	180	3400	34.4	3.65	1765	1154
Slab B5	706	180	3400	33.8	3.62	1765	1166

b =slab width; h =slab thickness; l =slab length; f_c^i =concrete compressive strength; f_t^i =concrete tensile strength; f_{pu} =specified tensile strength of tendon; f_{se} =effective stress in tendon.

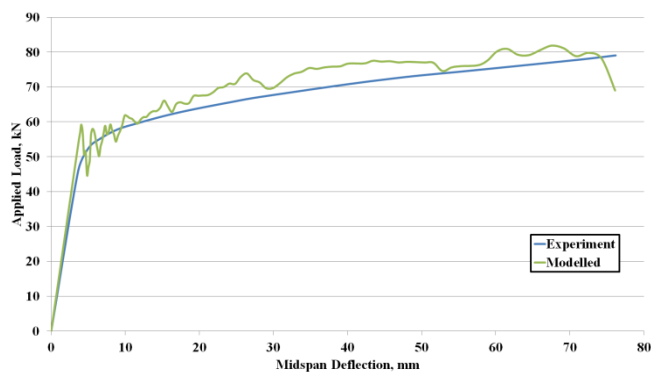


Fig. 3 Comparison of applied loads versus midspan deflection diagram of laboratory experiments with simulation of the Slab 5 specimen with unbonded tendons

In order to show the accuracy of present model for both selected slabs, the applied loads versus mid-span deflection diagram of the simulated specimens were compared with laboratory experiments, as displayed in Figs. 3 and 4.

As illustrated in Figs. 3 and 4, the results of both simulations with unbonded and bonded tendons had good agreement with other findings (Cooke *et al.* 1981). The fluctuations in the curves such as in Fig. 3 is due to the onset of crack appearance and advancement in the specimens.

Moreover, Figs. 5 and 6 show the crack patterns of present simulation in comparison with the experimental ones (Cooke *et al.* 1981). Accordingly, the crack patterns in the constant moment zone of both unbonded and bonded slabs are in good agreement. It is worth noting that in order to depict the crack zones of the simulation in Abaqus, Maximum Principle Plastic Strain was used. In the color images of all crack patterns, variation of strain is shown

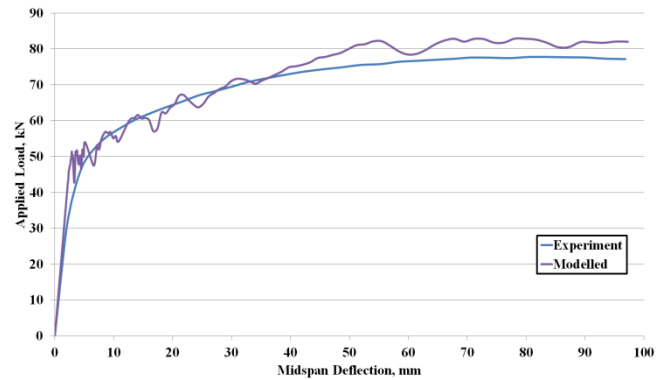


Fig. 4 Comparison of applied loads versus midspan deflection diagram of laboratory experiments with simulation of the Slab B5 specimen with bonded tendons

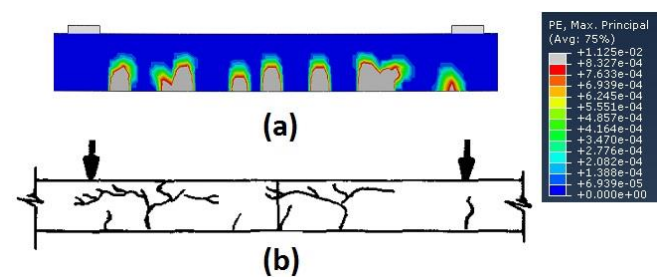


Fig. 5 Crack pattern in the constant moment zone of the Slab 5 specimen with unbonded tendons. (a) belongs to the simulation, and (b) belongs to laboratory experiment

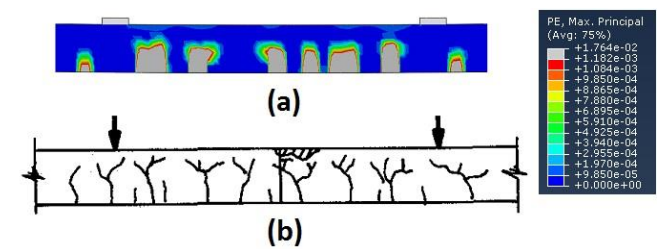


Fig. 6 Crack pattern in the constant moment zone of the Slab B5 specimen with bonded tendons. (a) belongs to the simulation, and (b) belongs to laboratory experiment

from maximum value in gray to a blue color which represents the undamaged concrete.

The simulated results corresponding to experimental work of Cooke *et al.* (1981), based on contact formulation method is presented here. Besides, the capability of this method in simulation of unbonded and bonded PT slabs and the change of strand bonding conditions from unbonded to bonded is verified. According to the results, the proposed method is highly efficient and powerful for the simulation of PT slabs and the change of strand bonding conditions. Also, the results of the simulation are consistent with the laboratory experiments of both unbonded and bonded slabs.

3.2 Four two-way unbonded PT slab-edge column connections

Table 2 describes the symbols employed for experimental (S) and modeled (M) samples which are used

Table 2 Symbols for experimental and modeled samples

Symbol	Parameters		Strand Bonding Conditions	
	f_c , MPa	Shear Cap	Unbonded	Bonded
S1	50.37	-	✓	-
M1U	50.37	-	✓	-
M1B	50.37	-	-	✓
M1UI	50.37	✓	✓	-
M1BI	50.37	✓	-	✓
M1UII	25	-	✓	-
M1BII	25	-	-	✓
M1UIII	25	✓	✓	-
M1BIII	25	✓	-	✓
S2	42.78	-	✓	-
M2U	42.78	-	✓	-
M2B	42.78	-	-	✓
M2UI	42.78	✓	✓	-
M2BI	42.78	✓	-	✓
M2UII	25	-	✓	-
M2BII	25	-	-	✓
M2UIII	25	✓	✓	-
M2BIII	25	✓	-	✓
S3	42.09	-	✓	-
M3U	42.09	-	✓	-
M3B	42.09	-	-	✓
M3UI	42.09	✓	✓	-
M3BI	42.09	✓	-	✓
M3UII	25	-	✓	-
M3BII	25	-	-	✓
M3UIII	25	✓	✓	-
M3BIII	25	✓	-	✓
S4	48.30	-	✓	-
M4U	48.30	-	✓	-
M4B	48.30	-	-	✓
M4UI	48.30	✓	✓	-
M4BI	48.30	✓	-	✓
M4UII	25	-	✓	-
M4BII	25	-	-	✓
M4UIII	25	✓	✓	-
M4BIII	25	✓	-	✓

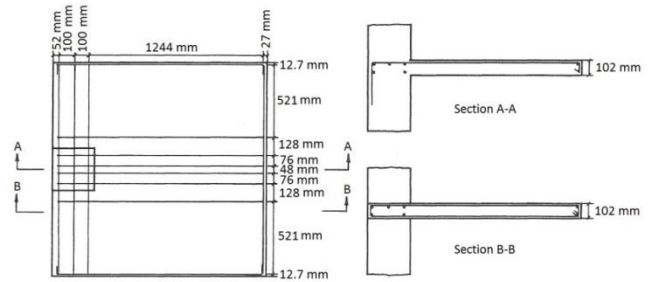


Fig. 7 Dimensions of slab and position of reinforcing bars (Sunidja *et al.* 1982)

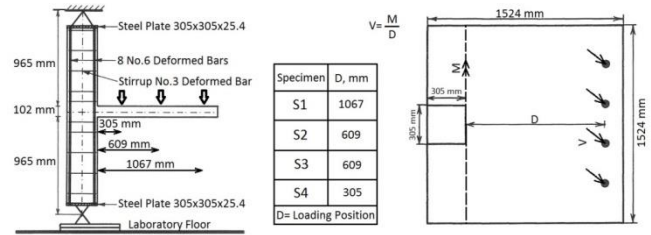


Fig. 8 Reinforcement in the column and different loading positions (Sunidja *et al.* 1982, Janghorban 2017)

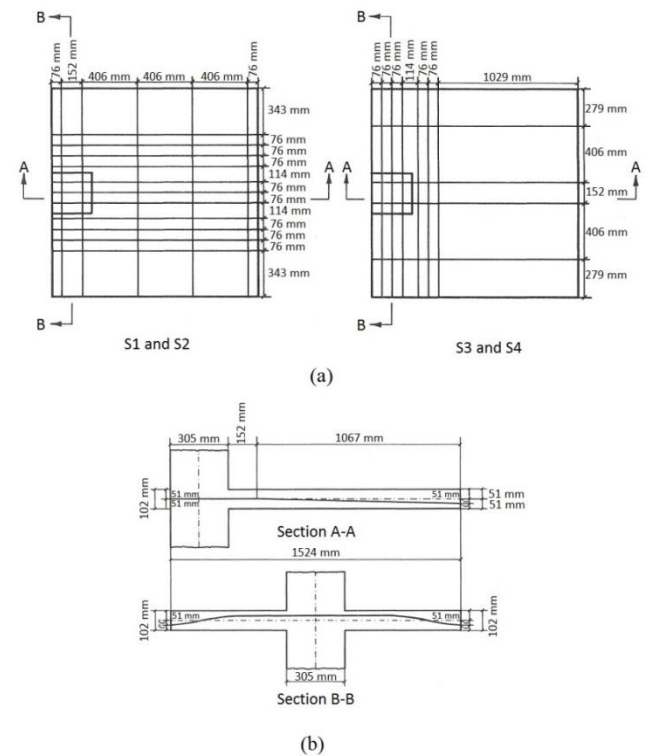


Fig. 9 (a) Tendons arrangement, and (b) Tendons profiles (Sunidja *et al.* 1982, Janghorban 2017)

in this study. *U* and *B* indicate the unbonded and bonded conditions.

This section provides the simulation of the four two-way unbonded PT slab-edge column connections tested by Sunidja *et al.* (1982). Fig. 7 display the dimensions of slabs and position of reinforcing bars. In all specimens, the reinforcing No. 3 bars with a diameter of 9.52 mm were positioned in the slabs.

Four specimens of Sunidja *et al.* (1982) called S1, S2, S3 and S4 were examined, which mainly differed in their loading positions. Different loading positions were selected to investigate the effect of moment shear ratio on the behavior of connections so that with the reduction of shear spans, the shear impact was maximized. All specimens underwent monotonic loading through four steel plates with a desired distance from the column until they failed. Fig. 8 presents the reinforcement in the column and different

loading positions. In the columns of all specimens, eight No. 6 bars with a diameter of 19.05 mm were used as longitudinal reinforcing bars to ensure that the flexural capacity of columns is larger than the slabs to avoid columns failure. Moreover, No. 3 bars were used as column stirrups.

All specimens only had hinge supports on the top and bottom of columns. The tendons arrangement of S1 and S2

Table 3 Properties and details used for simulation (Sunidja *et al.* 1982)

Parameter	Specimen				
	S1	S2	S3	S4	
f'_c , MPa	50.37	42.78	42.09	48.30	
f_r , MPa	5	4.32	4.84	4.33	
f_y , MPa	No. 3	501	501	501	
	No. 6	501	501	501	
f_u , MPa	No. 3	874	874	874	
	No. 6	830	830	830	
ε_y	No. 3	0.0025	0.0025	0.0025	
	No. 6	0.0025	0.0025	0.0025	
f_{pc} , MPa	W-E	4.48	4.76	1.80	1.82
	N-S	1.70	2.24	2.65	2.53
f_{pe} , MPa	W-E	1150.04	1223.13	1265.18	1285.18
	N-S	957.68	1265.18	1249.33	1194.17

f'_c =concrete compressive strength; f_r =modulus of rupture of concrete; f_y =yield stress of non-prestressed reinforcement; f_u =Maximum stress of non-prestressed reinforcement; ε_y =measured yield strain; f_{pc} =compressive stress in concrete; f_{pe} =compressive stress in concrete due only to effective prestressed forces. N-S= north to south; E-W=east to west. The east to west arrangement was used for loading spans.

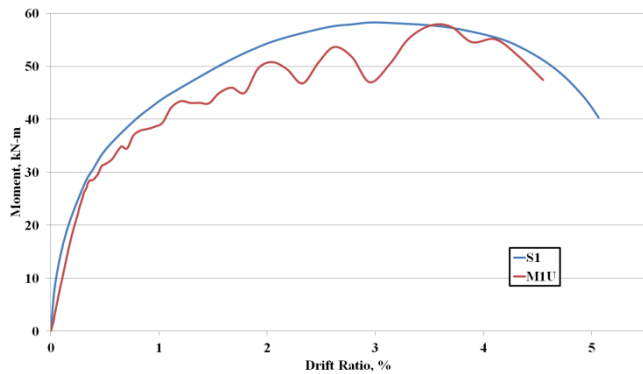


Fig. 10 Moment versus drift diagrams of S1 and M1U samples

specimens were banded from east to west and distributed from north to south. The tendons arrangement of S3 and S4 specimens were distributed from east to west and banded from north to south. Fig. 9 displays (a) tendons arrangement, and (b) tendons profiles. The tendons used in the specimens included grade 270 seven-wire strands with a diameter of 9.50 mm which were placed in 12.70 mm diameter polyethylene ducts.

The experimental properties and details which are used in this simulation are listed in Table 3 (Sunidja *et al.* 1982).

Figs 10, 11, 12 and 13 show the moment versus drift diagrams of simulation of the present study and the experiments on S1, S2, S3 and S4 specimens (Sunidja *et al.* 1982). They are in very good agreement.

Figs. 14, 15, 16 and 17 compare the crack patterns on the top surface of the simulated slabs with the crack patterns

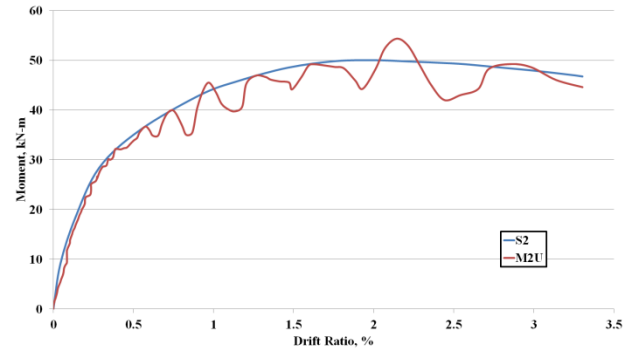


Fig. 11 Moment versus drift diagrams of S2 and M2U samples

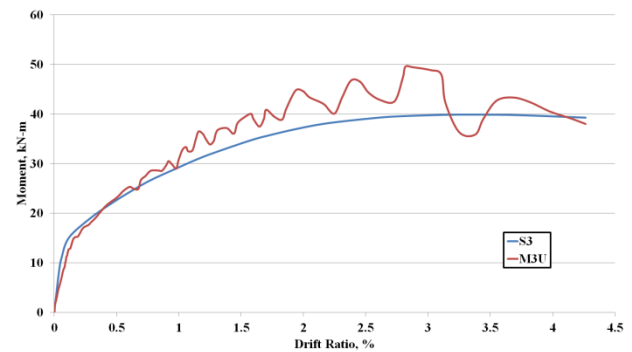


Fig. 12 Moment versus drift diagrams of S3 and M3U samples

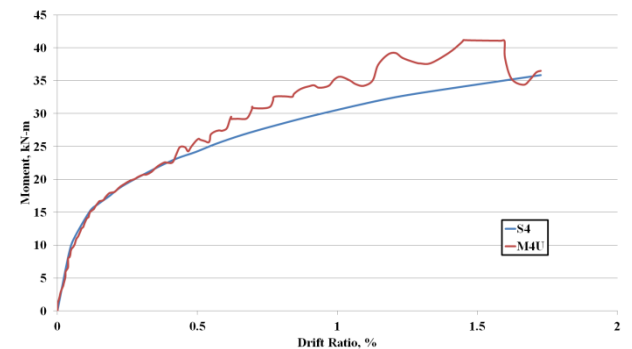


Fig. 13 Moment versus drift diagrams of S4 and M4U samples

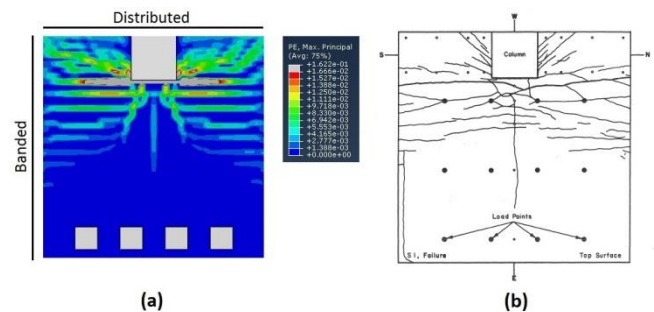


Fig. 14 Crack pattern on the top surface of slab at the connection failure step. (a) M1U, and (b) S1

on the top surface of the test slabs at failure step (Sunidja *et al.* 1982). According to the results, the crack positions of the simulated and test specimens were consistent.

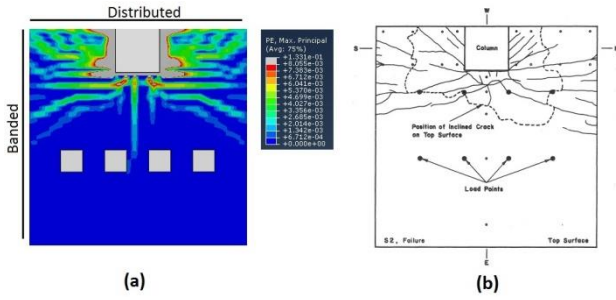


Fig. 15 Crack pattern on the top surface of slab at the connection failure step. (a) M2U, and (b) S2

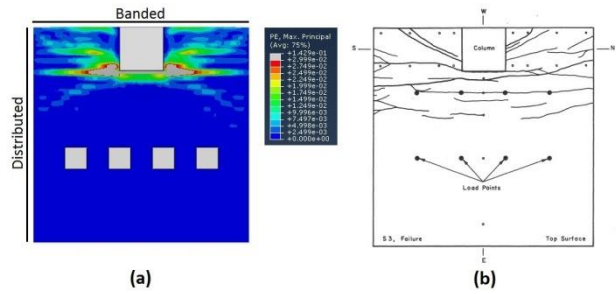


Fig. 16 Crack pattern on the top surface of slab at the connection failure step. (a) M3U, and (b) S3

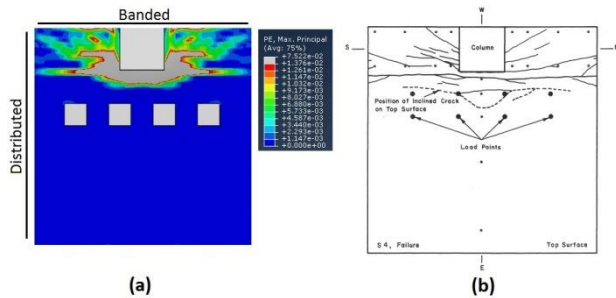


Fig. 17 Crack pattern on the top surface of slab at the connection failure step. (a) M4U, and (b) S4

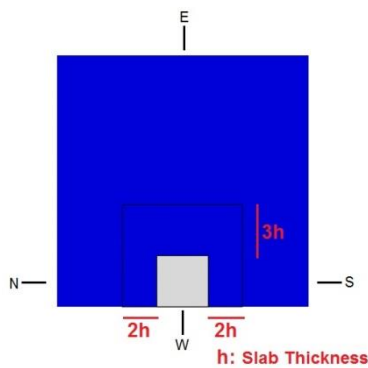


Fig. 18 Dimensions of the shear cap

According to the results of this section, the contact formulation method had an acceptable accuracy for the simulation of unbonded PT slab-edge column connections.

4. Parametric study of the numerical verification of PT slab-edge column connection

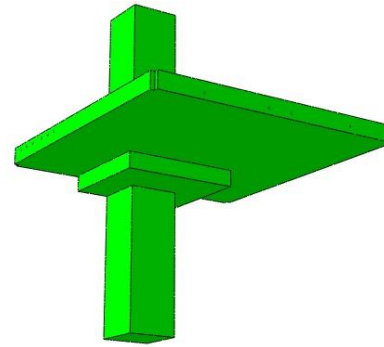


Fig. 19 Simulated PT slab-edge column connection with a shear cap

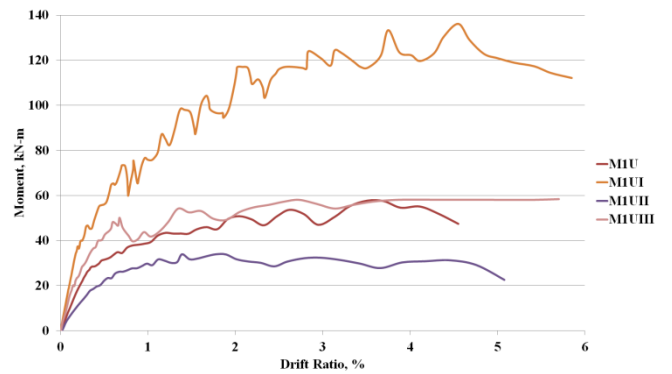


Fig. 20 The moment versus edge deflection diagram of M1U, M1UI, M1UII, and M1UIII specimens

In this section, reduction of concrete compressive strength, addition of a shear cap to the area of PT slab-edge column connections, and the change of strand bonding conditions from unbonded to bonded were investigated. To do so, moment versus drift diagrams, crack patterns, and verified Sunidja's data were employed.

4.1 Reduction of concrete compressive strength and addition of a shear cap to the area of PT slab-edge column connection

The concrete compressive strength of S1, S2, S3 and S4 specimens was reported to be 50.37, 42.78, 42.09 and 48.30 MPa respectively (Sunidja *et al.* 1982). In order to reduce the shear strength of connections, and to accelerate their shear failure, the concrete compressive strength was chosen to be 25 MPa for simulations.

There are several ways to increase the shear capacity of slab-column connections and prevent their shear failure caused by punching shear. One is making use of a shear cap to increase the slab thickness (h) in the area of slab-column connection. Fig. 18 presents the dimensions of the shear cap in detail. Fig. 19 displays one of the connections with a shear cap.

Figs. 20, 21, 22 and 23 display the moment versus drift diagrams of M1U, M2U, M3U and M4U specimens affected by the reduction of concrete compressive strengths and addition of a shear cap.

As shown in Figs. 20, 21, 22 and 23, the reduction of concrete compressive strength to 25 MPa, decreased the

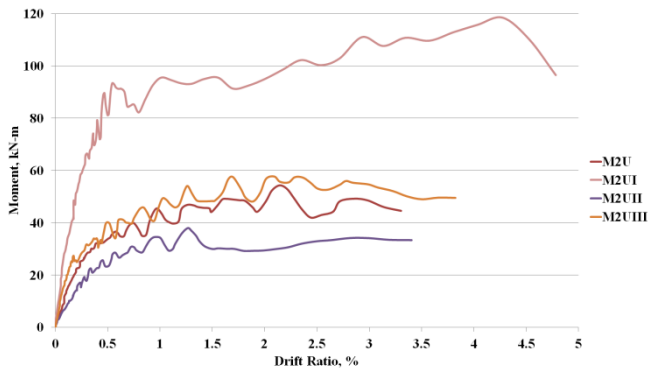


Fig. 21 The moment versus edge deflection diagram of M2U, M2UI, M2UII, and M2UIII specimens

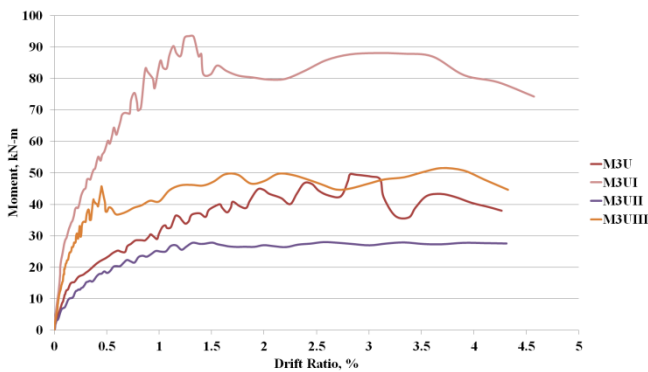


Fig. 22 The moment versus edge deflection diagram of M3U, M3UI, M3UII, and M3UIII specimens

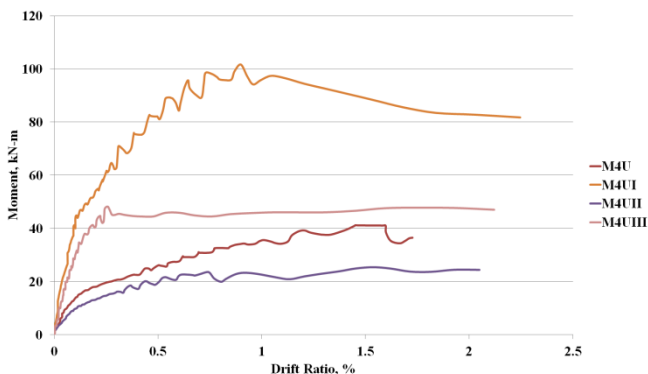


Fig. 23 The moment versus edge deflection diagram of M4U, M4UI, M4UII, and M4UIII specimens

flexural capacity of M1U, M2U, M3U and M4U specimens by 41%, 30%, 43% and 38% respectively. On the other hand, the addition of a shear cap increased the flexural capacity significantly. Table 4 presents the effect of addition of a shear cap on the increased flexural capacity of connections.

Presence of a shear cap in M1UIII, M2UIII, M3UIII and M4UIII specimens had a great impact on the flexural capacity of M3UIII and M4UIII specimens. The significant increase of flexural capacity in M3UIII and M4UIII specimens may contribute to their different tendons arrangement compared with the other two specimens as shown in Fig. 9. As mentioned before, the tendons arrangement of M3UIII and M4UIII was distributed in the

Table 4 Percentage of increased flexural capacity for different compressive strengths with unbonded tendons in the presence of a shear cap relative to the same specimens without a shear cap

Specimen	Increased Flexural Capacity %
M1UI relative to M1U	136
M1UIII relative to M1UII	72
M2UI relative to M2U	118
M2UIII relative to M2UII	52
M3UI relative to M3U	88
M3UIII relative to M3UII	84
M4UI relative to M4U	147
M4UIII relative to M4UII	87

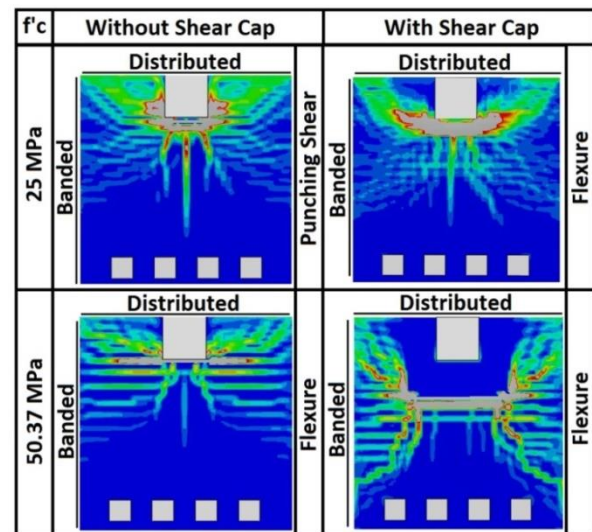


Fig. 24 Crack patterns on the top surface of slabs in M1U, M1UI, M1UII, and M1UIII specimens at the failure step of connections

direction of loading spans and banded in another direction, whereas tendons arrangement of M1UIII and M2UIII specimens was banded in the direction of loading spans and distributed in another direction.

Figs. 24, 25, 26 and 27 display the crack patterns on the top surface of slabs in M1U, M2U, M3U and M4U specimens affected by the reduction of concrete compressive strengths and addition of a shear cap at the failure step of connections. The color codes are similar to the ones shown in Figs. 14 to 17. In all figures, the tendons arrangement is shown on the left and top of each specimen, and the failure type of each specimen is shown on the right side. The failure is considered to be punching shear when the maximum plastic strains are around the column, and it is considered flexural when the maximum plastic strains are in an almost direct line in front of the column perpendicular to the loading span.

According to these figures, addition of a shear cap reinforced the shear strengths of connections, and converted the failure mode. Even though the addition of a shear cap did not have any significant effect on the failure type of connection in M2UIII specimen, it reduced the plastic strain around the column.

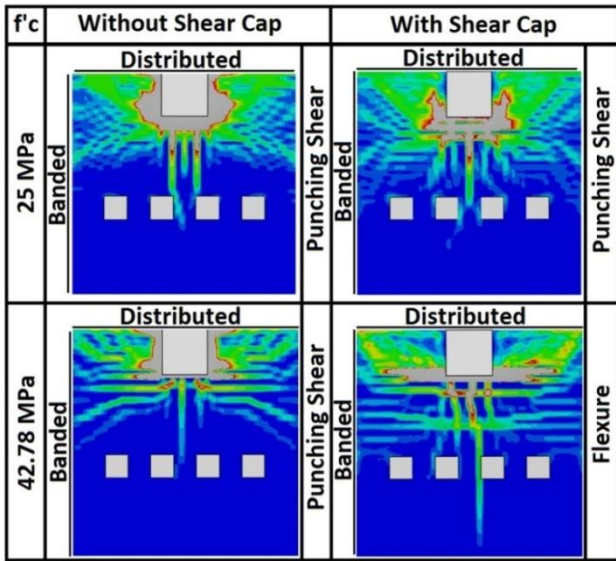


Fig. 25 Crack patterns on the top surface of slabs in M2U, M2UI, M2UII, and M2UIII specimens at the failure step of connections

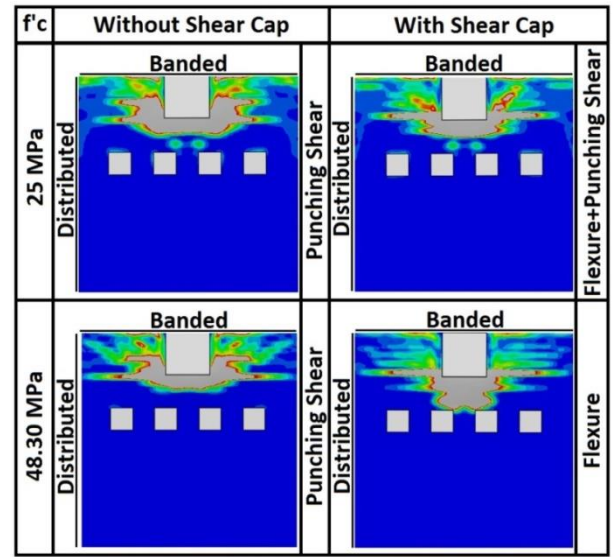


Fig. 27 Crack patterns on the top surface of slabs in M4U, M4UI, M4UII, and M4UIII specimens at the failure step of connections

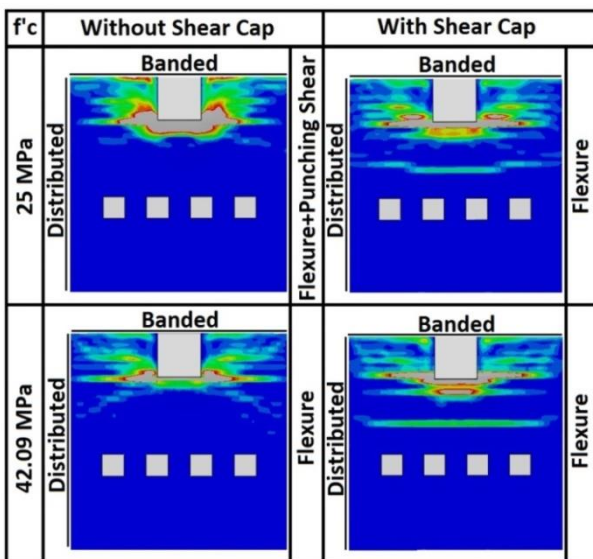


Fig. 26 Crack patterns on the top surface of slabs in M3U, M3UI, M3UII, and M3UIII specimens at the failure step of connections

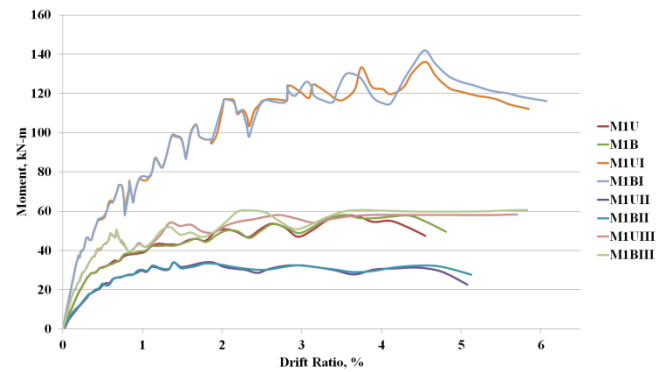


Fig. 28 The moment versus edge deflection diagram of M1U, M1B, M1UI, M1BI, M1UII, M1BII, M1UIII, and M1BIII specimens

Table 5 Increased flexural capacity % of modeled specimens with bonded tendons relative to the corresponding unbonded tendons

Specimen	Increased Flexural Capacity %
M1B relative to M1U	0.71
M1BI relative to M1UI	4.25
M1BII relative to M1UII	0.28
M1BIII relative to M1UIII	3.86
M2B relative to M2U	0.22
M2BI relative to M2UI	1.44
M2BII relative to M2UII	2.70
M2BIII relative to M2UIII	0.57
M3B relative to M3U	2.55
M3BI relative to M3UI	3.57
M3BII relative to M3UII	6.86
M3BIII relative to M3UIII	0.28
M4B relative to M4U	0.83
M4BI relative to M4UI	1.22
M4BII relative to M4UII	0.70
M4BIII relative to M4UIII	7.00

4.2 The change of strand bonding conditions from unbonded to bonded

Even though the bonded PT slabs are widely used in different places, fewer experiments have been done on this system compared to the unbonded PT slabs (Bondy 2012). Therefore, it was necessary to conduct a modeling approach to the performance of the bonded PT slabs. To do so, the strand bonding conditions of all numerical models, discussed in section 4.1, have been converted from unbonded to bonded in this work.

Fig. 28 displays the moment versus drift diagram of M1U and M1B specimens with/without a shear cap and different values of concrete compressive strengths.

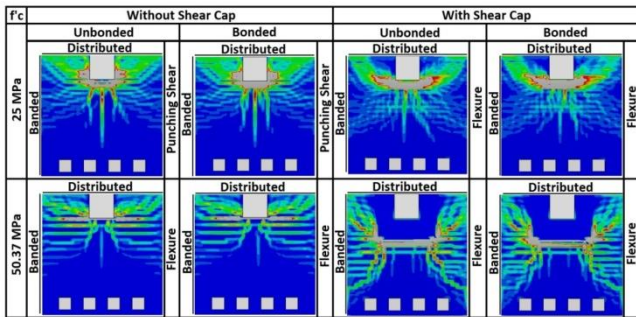


Fig. 29 Crack patterns on the top surface of the slabs in M1U, M1B, M1UI, M1BI, M1UII, M1BII, M1UIII, and M1BIII specimens at the failure step of connections

Similar moment versus drift ratio diagrams were obtained for M2U, M2B, M3U, M3B, M4U, and M4B specimens, which are not reported to avoid prolonging the article. Table 5 presents the percentage of increased flexural capacity of specimens with bonded tendons relative to the same specimens with unbonded tendons.

As shown in Fig. 28, the change of strand bonding conditions from unbonded to bonded had an insignificant effect on the flexural capacity of PT slab-edge column connections.

Fig. 29 displays the crack patterns on the top surface of slabs in M1U and M1B specimens with/without a shear cap and different values of concrete compressive strengths at the connection failure step. Similar crack patterns were analyzed for M2U, M2B, M3U, M3B, M4U, and M4B specimens, which are not reported to shorten the paper. Likewise the results of moment versus drift diagram (Fig. 28), the crack patterns did not have any significant changes in the failure type of connections by changing the strand bonding conditions. The distinction between the crack patterns of both tendons is associated with the crack paths and their severity.

Table 6 shows the failure modes of all 32 simulated cases in this study.

5. Conclusions

In this work, contact formulation method of FEA Abaqus software was employed to simulate the unbonded and bonded PT slabs. Effects of different components including concrete, reinforcing bars, and PT tendons were imposed. Besides, the relations of these components and application of PT force were considered. In practice, the experimental works of Sunidja *et al.* (1982) and Cooke *et al.* (1981) were simulated in order to verify the proposed modeling of PT slabs. Upon the consistency of the numerical results with the experimental test results, several problems were investigated for the first time on the lateral performance and failure of PT slab-edge column connections. These problems included the parametric effect of (a) strand bonding conditions, (b) presence and absence of a shear cap in the area of slab-column connections, and (c) change of concrete compressive strength.

The findings of the current study are outlined below:

Table 6 The type of connection failures in specimens with different values of concrete compressive strengths for unbonded and bonded tendons, with/without a shear cap

Specimen	Tendon Arrangement*		f_c (MPa)	Shear Cap	Strand Bonding Conditions	Type of Failure
	E-W	N-S				
M1U	banded	distributed	50.37	-	unbonded	flexure
M1B	banded	distributed	50.37	-	bonded	flexure
M1UI	banded	distributed	50.37	✓	unbonded	flexure
M1BI	banded	distributed	50.37	✓	bonded	flexure
M1UII	banded	distributed	25	-	unbonded	punching shear
M1BII	banded	distributed	25	-	bonded	punching shear
M1UIII	banded	distributed	25	✓	unbonded	flexure
M1BIII	banded	distributed	25	✓	bonded	flexure
M2U	banded	distributed	42.78	-	unbonded	punching shear
M2B	banded	distributed	42.78	-	bonded	punching shear
M2UI	banded	distributed	42.78	✓	unbonded	flexure
M2BI	banded	distributed	42.78	✓	bonded	flexure
M2UII	banded	distributed	25	-	unbonded	punching shear
M2BII	banded	distributed	25	-	bonded	punching shear
M2UIII	banded	distributed	25	✓	unbonded	punching shear
M2BIII	banded	distributed	25	✓	bonded	punching shear
M3U	distributed	banded	42.09	-	unbonded	flexure
M3B	distributed	banded	42.09	-	bonded	flexure
M3UI	distributed	banded	42.09	✓	unbonded	flexure
M3BI	distributed	banded	42.09	✓	bonded	flexure
M3UII	distributed	banded	25	-	unbonded	flexure+punching shear
M3BII	distributed	banded	25	-	bonded	flexure+punching shear
M3UIII	distributed	banded	25	✓	unbonded	flexure
M3BIII	distributed	banded	25	✓	bonded	flexure
M4U	distributed	banded	48.30	-	unbonded	punching shear
M4B	distributed	banded	48.30	-	bonded	punching shear
M4UI	distributed	banded	48.30	✓	unbonded	flexure
M4BI	distributed	banded	48.30	✓	bonded	flexure
M4UII	distributed	banded	25	-	unbonded	punching shear
M4BII	distributed	banded	25	-	bonded	punching shear
M4UIII	distributed	banded	25	✓	unbonded	flexure+punching shear
M4BIII	distributed	banded	25	✓	bonded	flexure+punching shear

*N-S= north to south; E-W= east to west. The east to west arrangement was used for loading span.

- The reduction of concrete compressive strength from 50.37, 42.78, 42.09 and 48.30 MPa to 25 MPa in the absence of a shear cap decreased the moment transfer capacity of M1U, M2U, M3U and M4U specimens by 41%, 30%, 43% and 38% respectively.
- The addition of a shear cap to M1U, M2U, M3U and M4U specimens increased the moment transfer capacity by 136%, 118%, 88% and 147% respectively.
- The addition of a shear cap to M1UII, M2UII, M3UII and M4UII specimens increased the moment transfer capacity by 72%, 52%, 84% and 87% respectively.
- Comparing the effect of the high concrete compressive strength versus the addition of a shear cap showed the latter had a higher shear capacity and converted the failure mode of connections from shear rigidity to flexural ductility. This issue highlights the fact that adding a shear cap instead of using a high concrete

compressive strength is more efficient.

- The use of a shear cap in the area of slab-column connections could significantly increase the shear capacity of connections.
- Based on the results of crack patterns, the cracks were flexural at the beginning, and upon the advancement, three types of flexural, punching shear and a combination of flexural and punching shear failures were developed which depend on the specimen conditions.
- Using a high concrete compressive strength with a shear cap, a flexural failure due to the significant presence of a high shear capacity of connections was exhibited.
- The change of strands bonding condition from unbonded to bonded in the PT slab-edge column connections had an inconsiderable effect on the flexural capacity and crack patterns of connections.

References

- Abdelatif, A.O., Owen, J.S. and Hussein, M.F.M. (2015), "Modeling the prestress transfer in pre-tensioned concrete elements", *Finite Elem. Anal. Des.*, **94**, 47-63.
- Abdullah, A.B.M., Rice, J.A., Hamilton, H.R. and Consolazio, G.R. (2016), "An investigation on stressing and breakage response of a prestressing strand using an efficient finite element model", *Eng. Struct.*, **123**, 213-224.
- ACI 318 (2014), Building Code Requirements for Structural Concrete and Commentary, American Concrete Institute; Farmington Hills, MI, USA.
- Bilý, P. and Kohoutková, A. (2017), "A numerical analysis of the stress-strain behavior of anchorage elements and steel liner of a prestressed concrete containment wall", *Struct.*, **12**, 24-39.
- Bondy, K.B. (2012), "Two-way post-tensioned slabs with bonded tendons", *PTI J.*, **8**(2), 43-48.
- Brunesi, E., Bolognini, D. and Nascimbene, R. (2015), "Evaluation of the shear capacity of precast-prestressed hollow core slabs: numerical and experimental comparisons", *Mater. Struct.*, **48**(5), 1503-1521.
- Carreira, D.J. and Chu, K.H. (1985), "Stress-strain relationship for plain concrete in compression", *ACI Proc.*, **83**(6), 797-804.
- Cooke, N., Park, R. and Yong, P. (1981), "Flexural strength of prestressed concrete members with unbonded tendons", *PCI J.*, **26**(6), 52-80.
- Devalapura, R.K. and Tadros, M.K. (1992), "Stress-strain modeling of 270 ksi low-relaxation prestressing strands", *PCI J.*, **37**(2), 100-106.
- Dilger, W.H. and Shatila, M. (1989), "Shear strength of prestressed concrete edge slab-column connections with and without shear stud reinforcement", *Can. J. Civil Eng.*, **16**(6), 807-819.
- Hajali, M., Alavinasab, A. and Shdid, C.A. (2015), "Effect of the location of broken wire wraps on the failure pressure of prestressed concrete cylinder pipes", *Struct. Concrete*, **16**(2), 297-303.
- Han, S.W., Kee, S.H., Park, Y.M., Lee, L.H. and Kang, T.H.K. (2006), "Hysteretic behavior of exterior post-tensioned flat plate connections", *Eng. Struct.*, **28**(14), 1983-1996.
- Huang, Y. (2012), "Finite element method for post-tensioned prestressed concrete structures", Ph.D. Dissertation, University of Oklahoma, Norman, USA.
- Huang, Y., Kang, T.H.K., Ramseyer, C. and Rha, C. (2010), "Background to multi-scale modeling of unbonded post-tensioned concrete structures", *Int. J. Theo. Appl. Multisc. Mech.*, **1**(3), 219-235.
- Hwang, J.W., Kwak, J.H. and Kwak, H.G. (2014), "Finite-element model to evaluate nonlinear behavior of posttensioned composite beams with partial shear connection", *J. Struct. Eng.*, **141**(8), 1-15.
- Janghorban, F. (2017), "Assessment of seismic performance of post-tensioned flat slab connections to edge column with consideration of strand bonding condition, existing of shear cap and concrete compressive strength", M.Sc. Dissertation, University of Tehran Kish International Campus, Kish, Iran.
- Kang, T.H.K. and Huang, Y. (2012), "Nonlinear finite element analyses of unbonded post-tensioned slab-column connections", *PTI J.*, **8**(1), 4-19.
- Kang, T.H.K., Huang, Y., Shin, M., Lee, J.D. and Cho, A.S. (2015), "Experimental and numerical assessment of bonded and unbonded post-tensioned concrete members", *ACI Struct. J.*, **112**(6), 735-748.
- Kim, U., Huang, Y., Chakrabarti, P.R. and Kang, T.H.K. (2014), "Modeling of post-tensioned one-way and two-way slabs with unbonded tendons", *Comput. Concrete*, **13**(5), 587-601.
- Kwak, H.G., Kim, J.H. and Kim, S.H. (2006), "Nonlinear analysis of prestressed concrete structures considering slip behavior of tendons", *Comput. Concrete*, **3**(1), 43-64.
- Martinez Cruzado, J.A. (1993), "Experimental study of post-tensioned flat plate exterior slab-column connections subjected to gravity and biaxial loading", Ph.D. Dissertation, University of California, Berkeley, USA.
- Mattock, A.H., Yamazaki, J. and Kattula, B.T. (1971), "Comparative study of prestressed concrete beams, with and without bond", *ACI Proc.*, **68**(2), 116-125.
- Nie, J., Tao, M., Cai, C.S. and Li, S. (2011), "Analytical and numerical modeling of prestressed continuous steel-concrete composite beams", *J. Struct. Eng.*, **137**(12), 1405-1418.
- Nilson, A.H., Darwin, D. and Dolan, C.W. (2009), *Design of Concrete Structures*, 14th Edition, McGraw Hill, New York, USA.
- Sunidja, H., Foutch, D.A. and Gamble, W.L. (1982), "Response of prestressed concrete plate-edge column connections", Report No. UILU-ENG-82-2006, Structural Research Series No. 498, University of Illinois at Urbana-Champaign.
- Trongtham, N. and Hawkins, N.M. (1977), "Moment transfer to columns in unbonded post-tensioned prestressed concrete slabs", Report No. SM77-3, Department of Civil Engineering, University of Washington at Seattle.
- Yapar, O., Basu, P.K. and Nordendale, N. (2015), "Accurate finite element modeling of pretensioned prestressed concrete beams", *Eng. Struct.*, **101**, 163-178.
- Zobel, R. and Curbach, M. (2017), "Numerical study of reinforced and prestressed concrete components under biaxial tensile stresses", *Struct. Concrete*, **18**(2), 356-365.

HK